Title	High-resolution photoelectron spectroscopy study of Kondo metals : SmSn3 and Sm0.9La0.1Sn3
Auther(s)	Yamaoka, Hitoshi; Thunström, Patrik; Jarrige, Ignace; Shimada, Kenya; Tsujii, Naohito; Arita, Masashi; Iwasawa, Hideaki; Hayashi, Hirokazu; Jiang, Jian; Habuchi, Takafumi; Hirayama, Daisuke; Namatame, Hirofumi; Taniguchi, Masaki; Murao, Urara; Hosoya, Shingo; Tamaki, Akira; Kitazawa, Hideaki
Citation	Physical Review B , 85 (11) : 115120
Issue Date	2012
DOI	10.1103/PhysRevB.85.115120
Self DOI	
URL	http://ir.lib.hiroshima-u.ac.jp/00033904
Right	(c) 2012 American Physical Society
Relation	

High-resolution photoelectron spectroscopy study of Kondo metals: $SmSn_3$ and $Sm_{0.9}La_{0.1}Sn_3$

Hitoshi Yamaoka,[1,*] Patrik Thunström,[2] Ignace Jarrige,[3] Kenya Shimada,[4] Naohito Tsujii,[5] Masashi Arita,[4] Hideaki Iwasawa,[4] Hirokazu Hayashi,[6] Jian Jiang,[6] Takafumi Habuchi,[6] Daisuke Hirayama,[6] Hirofumi Namatame,[4] Masaki Taniguchi,[4,6] Urara Murao,[7] Shingo Hosoya,[7] Akira Tamaki,[7] and Hideaki Kitazawa[5]

[1]*Harima Institute, RIKEN (The Institute of Physical and Chemical Research), Sayo, Hyogo 679-5148, Japan*
[2]*Department of Physics and Mathematical Science, Uppsala University, Box 530, SE-75121 Uppsala, Sweden*
[3]*Japan Atomic Energy Agency, SPring-8, Sayo, Hyogo 679-5148, Japan*
[4]*Hiroshima Synchrotron Radiation Center, Hiroshima University, Higashi-Hiroshima, Hiroshima 739-0046, Japan*
[5]*Quantum Beam Center, National Institute for Materials Science, 1-2-1 Sengen, Tsukuba 305-0047, Japan*
[6]*Graduate School of Science, Hiroshima University, Higashi-Hiroshima, Hiroshima 739-0046, Japan*
[7]*Tokyo Denki University, Hatoyama, Hiki, Saitama 350-0394, Japan*

(Received 21 November 2011; published 26 March 2012)

We performed a high-resolution photoelectron spectroscopy study on the Kondo metals $SmSn_3$ and $Sm_{0.9}La_{0.1}Sn_3$. The experimental results are compared with calculations of density of state performed within the local density approximation plus the dynamical mean-field theory. The theory is found to reproduce the experimental valence-band spectra well. In both $SmSn_3$ and $Sm_{0.9}La_{0.1}Sn_3$ the bulk Sm valence is nearly trivalent, with a small fraction of divalent component. Resonant photoelectron spectroscopy indicates a decrease in the Kondo effect in the diluted system $Sm_{0.9}La_{0.1}Sn_3$.

DOI: 10.1103/PhysRevB.85.115120 PACS number(s): 79.60.−i, 71.20.Eh, 71.27.+a

I. INTRODUCTION

Valence fluctuations in $4f$-electron systems have generated profound interest for the past four decades because they are usually linked with exotic physical phenomena, some of which ensue from the interplay between the Kondo effect and the Ruderman-Kittel-Kasuya-Yoshoda interaction. SmB_6[1,2] and compressed SmS[3] are well-known examples of Sm compounds with an intermediate-valence ground state composed of nonmagnetic Sm^{2+} ($4f^6$) and magnetic Sm^{3+} ($4f^5$). SmB_6 is the first compound for which the intermediate valence state was observed using x-ray absorption spectroscopy.[1] SmS undergoes a pressure-induced phase transition from a black Sm^{2+} phase to a golden phase with an intermediate valence, corresponding to a semiconducting to metal phase transition. SmS has a nonmagnetic ground state of $J = 0$ but shows a Van Vleck paramagnetic susceptibility, which arises from thermal excitation to the low-lying $J = 1$ level. These compounds are also well known as Kondo insulators or narrow-gap semiconductors; at high temperatures they can be described as localized independent f moments interacting with itinerant conduction electrons, whereas at low temperatures they develop narrow-gap related properties.

Among Sm compounds, $SmSn_3$ is the first discovered Sm-based dense (or heavy fermion) Kondo material.[4,5] The temperature dependence of the resistivity shows a minimum around 45 K typical of the Kondo effect, and for $T \leqslant 10$ K the resistivity rapidly decreases.[5] Antiferromagnetic ordering with $T_N = 11$–12 K was revealed by magnetic susceptibility.[6,7] The electronic specific heat coefficient shows the large value of $\gamma \sim 180$ mJ/(mol K^2), indicating heavy fermion behavior at low temperatures.[8] The specific heat does not show a simple Λ-type temperature dependence, as two sharp and one broad peaks were observed, at 9.3, 9.6, and 10.8 K, respectively.[5] Correspondingly, the resistivity showed anomalies around 8.6–9.4 and at 10.3 K.[9] While the peak in the specific heat at 10.8 K corresponds to the antiferromagnetic transition, the origin of the two other peaks in the specific heat has not been clarified yet, though multipole magnetic order was suggested.[5] In diluted systems these anomalous features in the specific heat have been found to grow weaker.[10] The temperature dependence of the resistivity of $La_{1-y}Sm_ySn_3$ ($0 \leqslant y \leqslant 0.177$) shows that the Kondo minimum develops around 10–15 K as one substitutes La for Sm.[4] Whereas resistivity features are influenced by the crystal electric field for $SmSn_3$, this was shown not to be the case for $La_{1-y}Sm_ySn_3$.

Knowledge of the ground-state electronic structure of valence-fluctuating materials is crucial to understanding their peculiar physical properties. In $SmSn_3$ one may expect a Sm^{3+} ground state similar to the high-pressure phase of SmS. However, the typical Kondo effect observed in the temperature dependence of the resistivity points to a possible weak valence fluctuation, especially at low temperatures. This stresses the importance of a direct measurement of the electronic structure of $SmSn_3$, which has not yet been reported. Furthermore, in Sm compounds the bulk Sm^{2+} multiplet structure has never been separated from the surface ones.

In this paper we report a detailed experimental and theoretical study of the electronic structure of $SmSn_3$, and of the diluted system $Sm_{0.9}La_{0.1}Sn_3$ for comparison. High-resolution photoelectron spectroscopy (PES) measurements were carried out in two incident photon energy regions, soft x-ray (SX) and ultraviolet (UV). We performed calculations of density of state (DOS) within the local density approximation (LDA) plus dynamical mean-field theory (DMFT). Our results show that La substitution to the Sm sites weakens the Kondo effect. The bulk and surface components of Sm^{2+} are clarified by comparing the experimental results with the LDA + DMFT calculations.

II. EXPERIMENTS AND CALCULATIONS

A. Experiments and analyses

Single crystals of $SmSn_3$ and $Sm_{0.9}La_{0.1}Sn_3$ were prepared in a molybdenum melting pot in vacuum using an induction

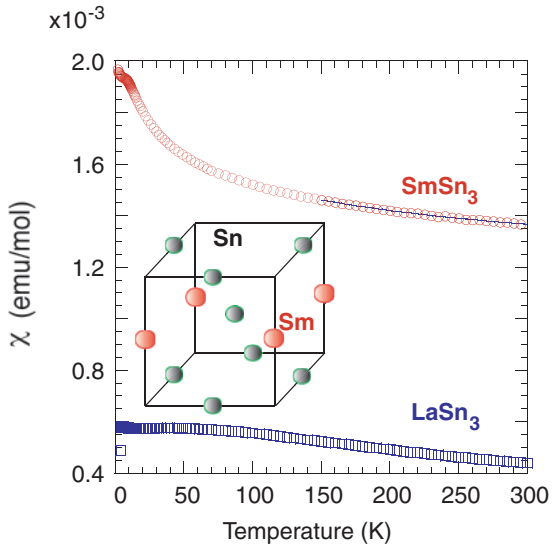

FIG. 1. (Color online) Magnetic susceptibility of $SmSn_3$ and $LaSn_3$ at 0.1 T as a function of temperature. The solid line for $SmSn_3$ is a fit with the modified Curie-Weiss law at $T \geqslant 150$ K. Inset: Schematic view of the crystal structure of $SmSn_3$.

furnace. $SmSn_3$ has a $AuCu_3$-type cubic crystal structure (space group $Pm3m$) with a lattice constant of 0.4685 nm.[5,7] A representation of the crystal structure is shown in Fig. 1. The Sm sites have a cubic point symmetry, $m3m$, while the Sn sites are located at a tetragonal point symmetry, $4/mmm$. The magnetic susceptibility was measured with a superconducting quantum interference device (SQUID) magnetometer at an applied field of 0.1 T. SX and UV PES measurements were performed at the undulator beamlines BL-1 and BL-9A at the Hiroshima Synchrotron Radiation Center HiSOR, equipped with high-resolution hemispherical electron-energy analyzers (R4000; VG-SCIENTA).[23,24] For UV PES the resolution (ΔE) was set to 10 meV at $h\nu = 16$ eV and 7 K. The vacuum pressure was better than 2×10^{-9} Pa during the measurements. In SX PES, ΔE was set to 40–50 meV around $h\nu = 136$ eV and 10 K. The vacuum pressure was better than 1×10^{-8} Pa. The Fermi edge of Au evaporated on the sample holders was used to calibrate the binding energy. All samples were fractured in vacuum just before the measurements. The energy resolution and the Fermi level were determined with a fit of the Fermi edge of Au using a convolution of a Gaussian and a Fermi-Dirac function.

B. Calculations

A fully charged self-consistent LDA + DMFT calculation[11,12] was performed, using the full-potential linear muffin-tin orbital code RSPt[13] and the DMFT implementation presented in Refs. 14–16. Strongly correlated Sm $4f$ states were treated with the Hubbard I approximation.[17,18] The local Coulomb interaction of the Sm $4f$ electrons was parameterized in terms of the Slater parameters F^0, F^2, F^4, and F^6. The parameters F^2, F^4, and F^6 were calculated at the beginning of each new LDA iteration through a radial integration of the unscreened local Coulomb interaction and then scaled by 0.92, 0.97, and 1.00, respectively. The scaling constants were set to account for the screening by the non-f-electrons. The final fully self-consistent values are $F^2 = 11.1$ eV, $F^4 = 7.2$ eV, and $F^6 = 5.3$ eV. The Hubbard U parameter F^0 cannot be calculated in the same way, as it is too heavily screened. Instead, it was set to the constant value of 7.0 eV. The **k** points were distributed in a $24 \times 24 \times 24$ Monkhorst-Pack grid, and Brillouin-zone integration was carried out using Fermi smearing with $T = 273$ K.

We note that the Hubbard I approximation does not take into account the hybridization effect between the correlated f orbitals and the bath and, therefore, cannot produce any quasiparticle peak associated with the Kondo effect. However, the multiplet spectrum derived from strongly localized $4f$ electrons is well reproduced by the Hubbard I approximation[16,19–21] and can therefore support the identification of these structures in the experimental data.

III. RESULTS AND DISCUSSION

A. Magnetic susceptibility

Figure 1 shows the magnetic susceptibility (χ) of $SmSn_3$ and $LaSn_3$ as a function of temperature. Assuming the modified Curie-Weiss law, we fit χ of $SmSn_3$ for $T \geqslant 150$ K to a function $\chi = C/(T + \Theta_p) + \chi_0 + \text{const.}$, where Θ_p and C are the Weiss temperature and Curie constant, respectively.[25] The Van Vleck term χ_0 is calculated to be $\chi_0 = \frac{N_A \mu_B^2}{k_B} \frac{20}{7\Delta E} = 0.000715$ emu/mol, where μ_B, N_A, and k_B are the Bohr magneton, the Avogadro's number, and the Boltzmann constant, respectively. ΔE ($\simeq$1400 K) is the energy difference of the lowest multiplets of $J = 5/2$ and $7/2$.[26] We note that our calculation taking into account the crystal field and spin-orbit coupling also shows a similar value of about 1600 K for ΔE.

C and Θ_p are estimated to be 0.076 and 130 K, respectively. Based on the formula $C = N_A {\mu_{\text{eff}}}^2/3k_B$, the effective magnetic moment is estimated to be $\mu_{\text{eff}} = 0.78\mu_B$, which is comparable to the Sm^{3+} ($4f^5$, $J = 5/2$) ion magnetic moment of $0.845\mu_B$ calculated with the formula according to Hund's rule, $\mu_{\text{eff}} = g\sqrt{J(J+1)}\mu_B$, where g is the Landé g factor. Thus, the high-temperature paramagnetic moment in $SmSn_3$ is mainly caused by Sm^{3+} ions, with the Van Vleck term and other constant term nearly corresponding to the susceptibility of $LaSn_3$. Similarly to SmS, where the Van Vleck paramagnetic susceptibility occurs due to thermal excitation to the low-lying $J = 1$ level, $SmSn_3$ also exhibits the Van Vleck susceptibility with a small Pauli-type contribution from Sm^{3+} ($4f^5$, ${}^6H_{5/2}$) states.[27]

B. LDA + DMFT calculations

Figure 2 shows the wide energy range calculations of the total [Fig. 2(a)], and partial and local [Figs. 2(b) and 2(c)] DOS of $SmSn_3$. A spectral line broadening of 0.01 Ry (0.136 eV) was used to compare the calculation with the experimental results in a wide binding energy range. In Fig. 2(b) the structures from $E_b = 0$ to 5 eV and from $E_b = 5$ to 11 eV correspond to Sm^{2+} and Sm^{3+} components, respectively.[22] Sn $5p$ states have a broad peak around $E_b = 2$–3 eV. Figures 2(d) and 2(e) show the detailed calculations near the Fermi level

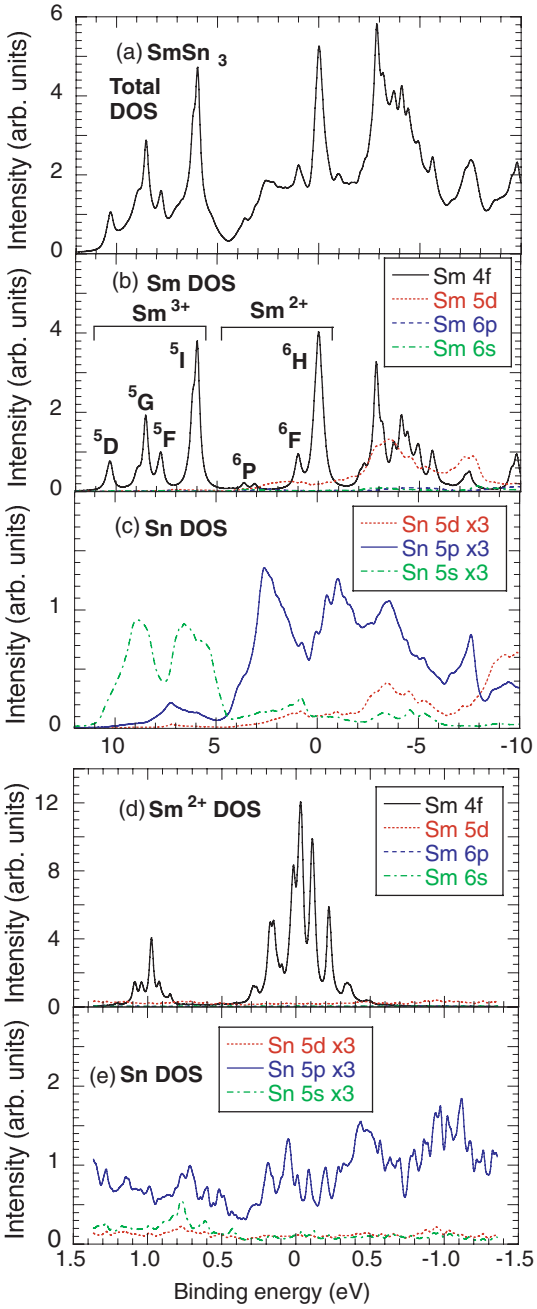

FIG. 2. (Color online) Result of the DOS calculated with LDA + DMFT with a spectral line broadening of 0.01 Ry (0.136 eV) for $SmSn_3$. (a) Total DOS. (b) Sm $4f$, $5d$, $6p$, and $6s$ partial DOS at $E_b \leqslant 12$ eV. (c) Sn $5d$, $5p$, and $5s$ partial DOS at $E_b \leqslant 12$ eV. Detailed partial DOS with a spectral line broadening of 0.001 Ry (0.0136 eV) near E_F for Sm (d) and Sn (c) at $E_b \leqslant 1.5$ eV. Note that in (c) and (d) the vertical scales are changed.

with a spectral line broadening of 0.001 Ry (0.0136 eV). These calculations show fine structures for both ^{6}F and ^{6}H lines of the Sm^{2+} component. We note that the ^{6}H component is spread across the Fermi level. For comparison with the PES spectra, we should take into account the incident energy dependence of the photoionization cross sections.

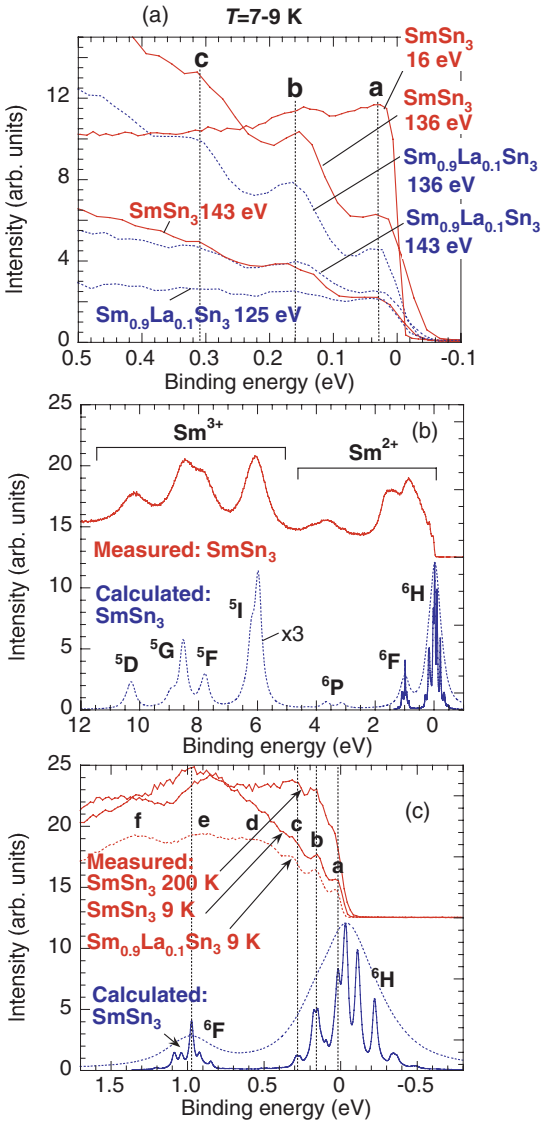

FIG. 3. (Color online) (a) Fine structure of the valence-band spectra near the Fermi level. (b) Comparison of the calculation of the DOS with the LDA + DMFT approximation with a spectral line broadening of 0.01 Ry (0.136 eV; dashed line) with the measured spectrum at 136 eV for $SmSn_3$. Detailed calculation with a spectral line broadening of 0.001 Ry (0.0136 eV; solid line) is also shown. (c) Enlargement of Fig. 3(b) near E_F with measured spectra of $SmSn_3$ and $Sm_{0.9}Ls_{0.1}Sn_3$ at 136 eV and 9 K with a spectrum of $SmSn_3$ at 143 eV and 200 K.

C. Origin of fine structures near E_F

Figure 3(a) shows near-E_F photoelectron spectra of $SmSn_3$ and $Sm_{0.9}La_{0.1}Sn_3$ measured at $h\nu = 16, 125, 136$, and 143 eV. Note that the incident photon energies of $h\nu = 136$ and 143 eV are in the energy range of the Sm $4d$-$4f$ resonance and that the Sm $4f$ intensity is accordingly enhanced, as described in detail in Sec. III E. Peaks a and b are clearly observed at all incident energies, and peak c at 136 and 143 eV. In Figs. 3(b) and 3(c) we show the theoretical Sm local DOS given by the LDA + DMFT calculation for $SmSn_3$ compared with the spectrum measured for $Sm_{0.9}La_{0.1}Sn_3$ at $h\nu = 136$ eV. The multiplets of both Sm^{3+} and Sm^{2+} components agree

very well with the calculated $SmSn_3$ spectrum as shown in Figs. 3(b) and 3(c), respectively. The detailed comparison in Fig. 3(c) allows us to identify the peaks in the experimental spectrum labeled a, b, c, and e as bulk ^6H and ^6F components of Sm^{2+}, respectively.[22] To our knowledge, UV and SX-PES spectra with resolved bulk components have not been reported for a Sm compound so far. In the detailed calculation the energy separation between peaks a, b, and c is of the order of 0.13 eV, which is much larger than the experimental energy resolution and, therefore, explains why we were able to clearly resolve them.

Based on the results of the first principle calculations,[29] the energy shifts of the surface components from the bulk ones should be 0.4–0.5 eV. Thus the broad peaks labeled d and f are probably derived from the surface contributions, similarly to what we previously observed in Yb compounds.[28] According to the calculated spectrum in Fig. 3(b), the ^6P components of Sm^{2+} are expected to appear within an electron binding energy range of $E_b = 3$–4 eV. Based on the fact that the calculated ^6P features have a very weak intensity, we can reasonably consider that the broad peak observed in the experimental spectrum around $E_b = 4$ eV mostly corresponds to the surface contribution of ^6P. We additionally note that the energy difference between the d and the f peaks is about 20% smaller than that between a and e, which reflects the different chemical environment.

D. Temperature dependence of the electronic structure near E_F

Figure 4(a) shows the temperature-dependent high-resolution valence-band spectra of $SmSn_3$ measured at $h\nu = 16$ eV. We observe two distinct features, which correspond to peaks a and b in Fig. 3. We note that in this incident photon energy range the photoionization cross section of $4f$ is one order smaller than that of Sn $5p$,[30] which results in a weaker contribution of the Sm^{2+} $4f$ states to the valence-band spectrum than the spectra measured at $h\nu = 136$ and 143 eV.

The temperature dependence of the DOS of $SmSn_3$ derived by dividing the valence-band spectra with a Gaussian-broadened Fermi-Dirac distribution is plotted in Fig. 4(b). One may examine the DOS down to $-5k_BT$.[31] A finite DOS exists from room temperature down to 6.8 K, which reflects the metallic character of $SmSn_3$. A V-shaped gap

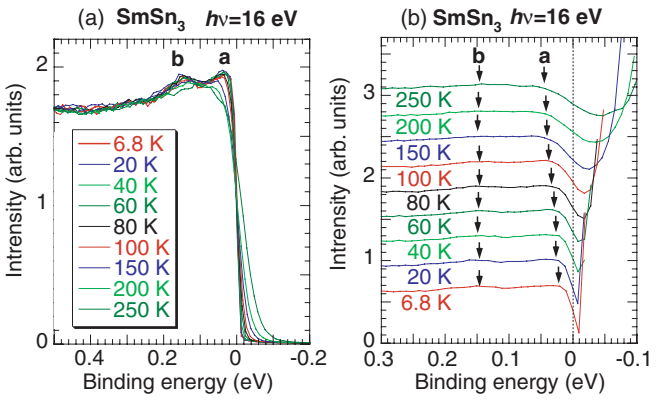

FIG. 4. (Color online) (a) Temperature dependence of valence-band spectra for $SmSn_3$ at $h\nu = 16$ eV. Two distinct peaks are labeled a and b. (b) Density of states near the Fermi level.

structure is observed just above the Fermi level in the entire measured temperature range. In $SmSn_3$ the ground state is a Γ_8 quadruplet and the energy difference between Γ_8 and the Γ_7 doublet is about 50 K.[32] Our calculation also gives a similar value of 45 K for the energy difference between Γ_8 and Γ_7. The stable gap position below 60 K in $SmSn_3$ likely corresponds to the fact that the system is in the Γ_8 ground state. Both the gap width and the binding energy of peak a decrease monotonically with decreasing temperature. Whereas the decrease in the gap at low temperatures is reminiscent of the metallic phase of FeSi before the transition to the insulator state,[33] the resistivity of $SmSn_3$ does rapidly decrease at low temperatures, ruling out a metal-to-insulator transition. There should exist a hybridization between the Sm $4f$ and the Sn $5p$ states. However, the Hubbard I approximation used in the LDA + DMFT calculation neglects this hybridization, so further theoretical study may be necessary to understand the temperature dependence of the DOS near E_F.

As mentioned above, the specific heat was reported to show a broad peak at 10.8 K and two sharp peaks at 9.3 and 9.6 K.[5] The two sharp peaks below T_N have been suggested to originate from multiple magnetic order such as quadrupole order.[34] Recently, a zero-field muon spin relaxation measurement for the analogue compound $SmIn_3$, which also showed anomalies in the specific heat at 16.5, 15.1, and 14.7 K,[5] indicated that the primary order parameters in all the ordered phases were magnetic, though the results were in contrast to the pure quadrupole ordering scenario.[34] Our PES data show little difference in the valence-band spectra between $T = 6.8$ and $T = 20$ K. This indicates that the electronic structure at E_F does not change significantly below 60 K.

E. Incident energy dependence

Figures 5(a) and 5(b) show the valence-band spectra for $E_b \leqslant 9$ eV and near the Fermi level, respectively, at $h\nu = 13$–21 eV. Figure 5(c) exhibits the contour intensity map of the spectra. We observe two kinds of peak features, labeled P1 and P2 in Fig. 5(a), which shift with the incident photon energies, while peaks a and b in Fig. 5(b) stay at a constant binding energy. As shown in Fig. 5(d) the energy of peak P2 shows a linear, slope 1 shift with the incident energy; we therefore assign it to the resonant Auger component. On the other hand, the incident energy dependence of the binding energy of peak P1 is much weaker.

We performed resonant PES[28,35] for incident photon energies of 136 and 143 eV. Figures 6(a) and 6(b) show examples of the fit of the valence-band spectrum of $SmSn_3$ at $h\nu = 143$ eV after subtracting the background. It is known that in the incident photon energy range of the Sm $4d$-$4f$ resonance, the Sm^{2+} component mainly originates from the surface layer. Consequently, the Sm^{2+} surface state is probed at these photon energies,[36,37] whereas the Sm^{3+} component is considered to be from the bulk even at these incident energies. At the surface the Sm atoms are less coordinated; their cohesive energy is therefore lower than that of the bulk Sm atoms, which results in the surface Sm atoms tending to be in the divalent state. However, in our high-resolution measurement we successfully separated a small bulk component of Sm^{2+}, as illustrated in Fig. 6(f). The bulk valence of $SmSn_3$ at 9 K is estimated from

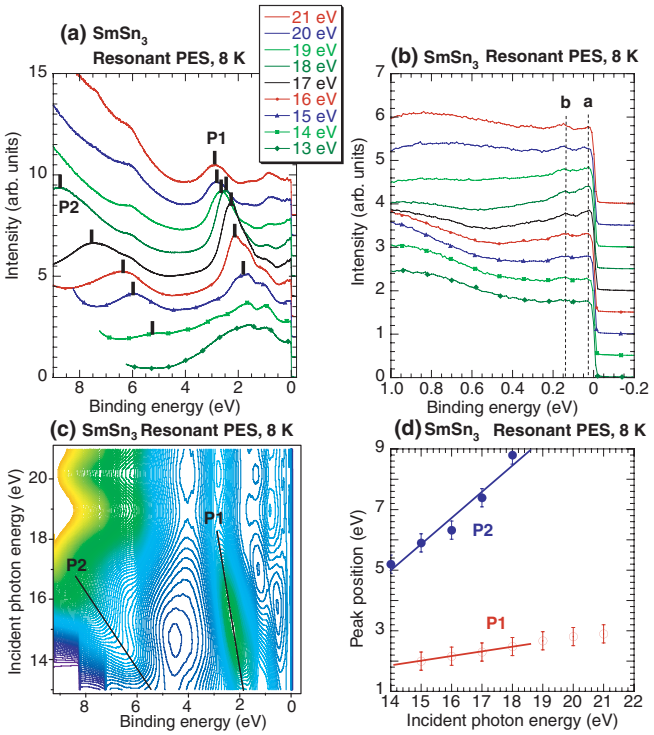

FIG. 5. (Color online) (a) Resonant photoelectron spectra of the valence band for $SmSn_3$ at $h\nu = 13$–21 eV. (b) Enlargement of (a) near the Fermi level. (c) Contour intensity map as a function of incident photon energies. (d) Peak energy positions of P1 (open circles) and P2 (filled circles) as a function of incident photon energies.

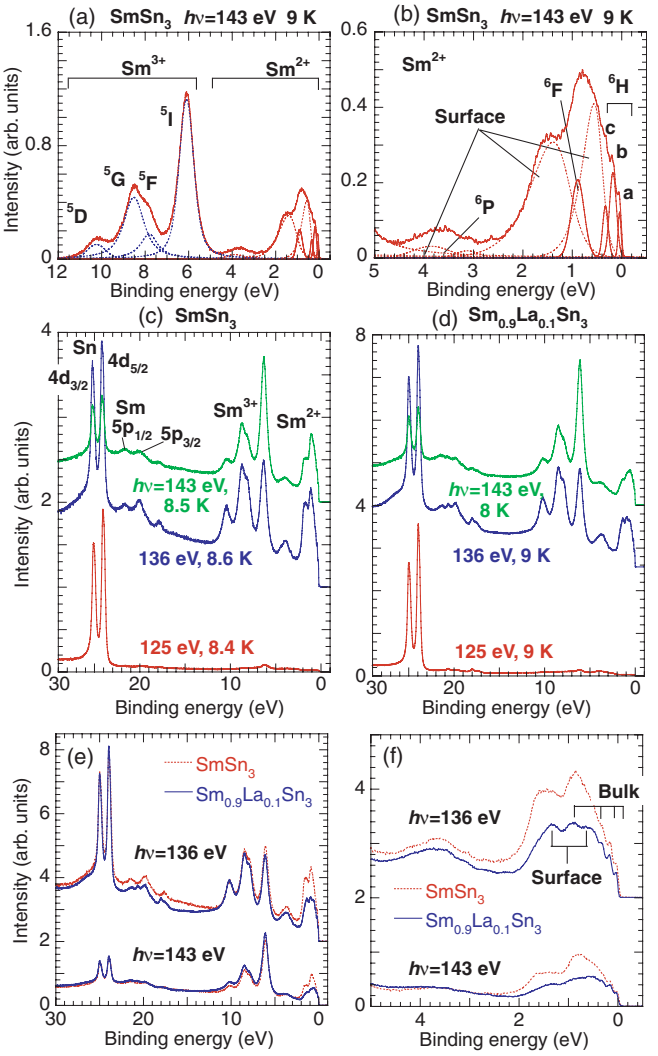

FIG. 6. (Color online) (a) Assignment of each line and an example of the fit for the spectrum of $SmSn_3$ at 9 K and $h\nu = 143$ eV after extracting the background. (b) Enlargement of the Sm^{2+} part in (a). (c) Resonant photoelectron spectra of the valence band for $SmSn_3$ at $h\nu = 136$ and 143 eV with the off-resonant spectrum at $h\nu = 125$ eV around 8.4–8.6 K. (d) Resonant photoelectron spectra of the valence band for $Sm_{0.9}La_{0.1}Sn_3$ at $h\nu = 136$ and 143 eV with the off-resonant spectrum at $h\nu = 125$ eV at 8–9 K. (e) Comparison of the valence-band spectra between $SmSn_3$ and $Sm_{0.9}La_{0.1}Sn_3$ at $h\nu = 136$ and 143 eV. (f) Enlargement of the spectra in (e) near the Fermi level.

the fits shown in Fig. 6(a) to be 2.93 ± 0.01. This result agrees with the magnetic susceptibility measurement, from which a Sm valence of nearly $3+$ was deduced.

Figures 6(c) and 6(d) show the PES spectra collected around the Sm $4d$-$4f$ resonance for $SmSn_3$ and $Sm_{0.9}La_{0.1}Sn_3$, along with the off-resonant spectra measured at $h\nu = 125$ eV. These spectra are normalized in intensity to the maximum of the Sn $4d$ peaks. The Sm $4f$ states are clearly observed due to both the high $4f$ photoionization cross section[30] and the $4d$-$4f$ resonance. In the off-resonant spectra the intensity is weak, and almost-flat spectral features are mainly derived from the Sn $5s$, $5p$, and $5d$ states as shown in Fig. 2(c). The weak peak around 7 eV may originate from the Sm^{3+} state. The difference between the on- and the off-resonant spectra should yield a residual spectrum that contains only the Sm states. We compare the spectra between $SmSn_3$ and $Sm_{0.9}La_{0.1}Sn_3$ at $h\nu = 136$ and 143 eV as shown in Figs. 6(e) and 6(f). The surface Sm^{2+} component in $Sm_{0.9}La_{0.1}Sn_3$ slightly shifts toward the Fermi level as shown in Fig. 6(f), corresponding to a chemical shift caused by La substitution. The intensities of both bulk and surface Sm^{2+} components for $Sm_{1-x}La_xSn_3$ are weaker than those for $SmSn_3$. This fact corresponds to the behavior of the temperature dependence of the resistivity; the feature of the Kondo minimum is weaker with increasing La concentration in $Sm_{1-x}La_xSn_3$ ($0.823 \leqslant x \leqslant 1$).[4] Furthermore, in a diluted system of $Sm_{1-x}La_xSn_3$ ($0 \leqslant x \leqslant 1$) the anomalous features in the specific heat grew weaker with the La substitution to the Sm site.[10] Our results indicate that La substitution to the Sm site weakens the Kondo effect.

Figures 7(a) and 7(b), respectively, show the valence-band spectra measured at $h\nu = 143$ eV on $SmSn_3$ and $Sm_{0.9}La_{0.1}Sn_3$ at 8–9 and 100 K. The spectral intensity is normalized to the area of Sn $4d$ peaks (not shown here). In $SmSn_3$ the intensity of both the bulk and the surface states of Sm^{2+} is stronger at 9 K than 100 K. This points to an enhancement of the valence fluctuations at low temperatures, hinting at a strengthening of the c-f hybridization.[38] Comparatively, the temperature-induced change in the spectrum of $Sm_{0.9}La_{0.1}Sn_3$ is smaller. This result is consistent with the weaker, diluted Kondo effect in $Sm_{0.9}La_{0.1}Sn_3$ compared with $SmSn_3$.

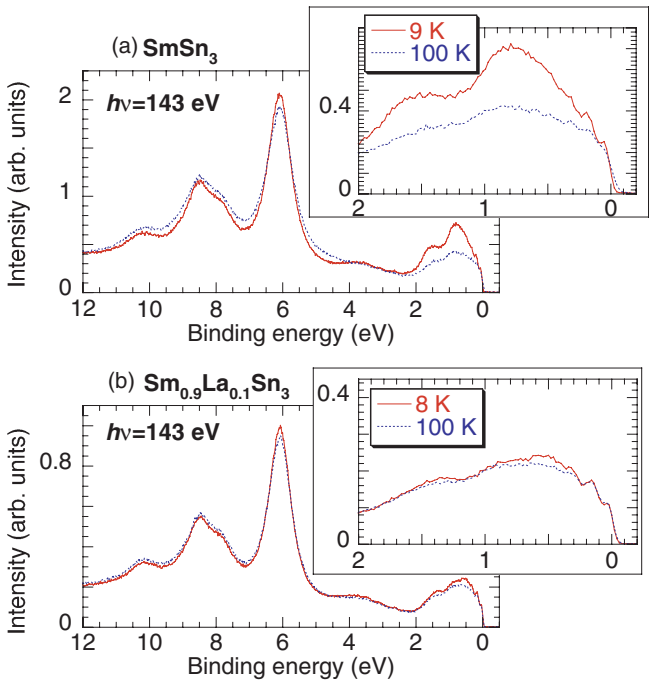

FIG. 7. (Color online) (a) Valence-band spectra for $SmSn_3$ at $h\nu = 143$ eV at 9 and 100 K. (b) Valence-band spectra for $Sm_{0.9}La_{0.1}Sn_3$ at $h\nu = 143$ eV at 8 and 100 K.

Finally, we consider the surface effect in $SmSn_3$ again. In $SmSn_3$ the inelastic mean free path of the photoelectrons is estimated to be of the order of 0.8 nm at $h\nu = 143$ eV, which is nearly twice the lattice constant of 0.4685 nm.[39] The value of the mean free path indicates that the Sm^{2+} component mainly arises from the surface layer at $h\nu = 143$ eV. Actually, at room temperature the surface to bulk spectral weight, $w_B = \exp\{-s/(\lambda_e \cos\theta)\}$, is estimated to be about 0.8, where s, λ_e, and θ are the thickness of the surface layer, the inelastic mean free path of the photoelectrons, and the emission angle from the surface normal, respectively.[40,41] In our case the thickness of the surface layer is estimated to be about $s = 0.13$ nm, which is 30% of the lattice constant and comparable to the case for Sm_4As_3 at $h\nu = 220$ eV.[40] These estimations also indicate that the weak bulk component is detectable as described above even in Sm^{2+} spectra measured around $h\nu = 143$ eV.

IV. CONCLUSION

We measured high-resolution photoelectron spectra on $SmSn_3$ and $Sm_{0.9}La_{0.1}Sn_3$ using both UV and SX incident photon energies. The UV PES spectra of $SmSn_3$ show a finite DOS at E_F, in agreement with the metallic character of the compound. The LDA + DMFT calculations reproduce the experimental valence-band spectra well, even the fine structures observed near E_F at a binding energy of <2 eV. We successfully distinguished the bulk and surface components of Sm^{2+} by comparing the experimental results with the LDA + DMFT calculations. Our results show that the electronic structure of $SmSn_3$ in the vicinity of E_F does not change much below 20 K, where the specific heat showed anomalous features. The PES and magnetic susceptibility results show that in $SmSn_3$ the bulk Sm valence is nearly trivalent, with a small fraction of Sm^{2+} component. In $SmSn_3$ the bulk components of both Sm^{2+} and Sm^{3+} show a temperature dependence, which we interpret as arising from an enhancement of the c-f hybridization at low temperatures. In comparison, the valence-band spectrum of $Sm_{0.9}La_{0.1}Sn_3$ shows a smaller temperature dependence, suggesting that the La substitution to the Sm sites weakens the Kondo effect.

ACKNOWLEDGMENTS

The experiments were performed at HiSOR beamlines BL-1 and BL-9A (HiSOR under Proposal No. 10-A-47) at Hiroshima University. We thank the N-BARD, Hiroshima University, for supplying the liquid helium. P.T. acknowledges financial support from the Swedish Research Council (VR) and Energimyndigheten (STEM). Calculations were performed at the Swedish national computer centers UPPMAX and NSC. This work was partly supported by Grants in Aid for Scientific Researches (Grants No. 22540343 and No. 22340103) from the Japan Society for the Promotion of Science in Japan.

*yamaoka@spring8.or.jp

[1] E. E. Vanstein, S. M. Blokhin, and Yu. B. Paderno, Sov. Phys. Solid State **6**, 281 (1965).
[2] E. Beaurepaire, J. P. Kappler, and G. Krill, Phys. Rev. B **41**, 6768 (1990).
[3] M. B. Maple and D. Wohlleben, Phys. Rev. Lett. **27**, 511 (1971).
[4] S. Bakanowski, J. E. Crow, and T. Mihalisin, Solid State Commun. **22**, 241 (1977).
[5] M. Kasaya, B. Liu, M. Sera, T. Kasuya, D. Endoh, T. Goto, and T. Fujimura, J. Magn. Magn. Mater. **52**, 289 (1985).
[6] T. Tsuchida and W. E. Wallace, J. Chem. Phys. **43**, 3811 (1965).
[7] H. W. Wijn, A. M. van Diepen, and K. H. J. Buschow, Phys. Rev. B **7**, 524 (1977).
[8] T. Kasuya, M. Kasaya, K. Takegahara, F. Iga, B. Liu, and N. Kobayashi, J. Less-Common Met. **127**, 337 (1987).
[9] Z. Kletowski, Solid State Commun. **62**, 745 (1987).
[10] U. Murao, K. Morita, S. Hashio, Y. Kawamura, A. Kikkawa, H. S. Suzuki, H. Kitazawa, and A. Tamaki (unpublished).
[11] A. Georges, G. Kotliar, W. Krauth, and M. J. Rozenberg, Rev. Mod. Phys. **68**, 13 (1996).
[12] G. Kotliar, S. Y. Savrasov, K. Haule, V. S. Oudovenko, O. Parcollet, and C. A. Marianetti, Rev. Mod. Phys. **78**, 865 (2006).
[13] J. Wills, O. Eriksson, M. Alouani, and D. Price, in *Electronic Structure and Physical Properies of Solids*, edited by H. Dreysse (Springer, New York, 2000), pp. 148–167.
[14] A. Grechnev, I. Di Marco, M. I. Katsnelson, A. I. Lichtenstein, J. Wills, and O. Eriksson, Phys. Rev. B **76**, 035107 (2007).
[15] I. Di Marco, J. Minár, S. Chadov, M. I. Katsnelson, H. Ebert, and A. I. Lichtenstein, Phys. Rev. B **79**, 115111 (2009).

[16]P. Thunström, I. Di Marco, A. Grèchnev, S. Lebegue, M. I. Katsnelson, A. Svane, and O. Eriksson, Phys. Rev. B **79**, 165104 (2009).
[17]J. Hubbard, Proc. R. Soc. London Ser. A **276**, 238 (1963).
[18]A. I. Lichtenstein and M. I. Katsnelson, Phys. Rev. B **57**, 6884 (1998).
[19]S. Lebègue, G. Santi, A. Svane, O. Bengone, M. I. Katsnelson, A. I. Lichtenstein, and O. Eriksson, Phys. Rev. B **72**, 245102 (2005).
[20]S. Lebègue, A. Svane, M. I. Katsnelson, A. I. Lichtenstein, and O. Eriksson, J. Phys. Condens. Matter **18**, 6329 (2006).
[21]O. Grånäs, I. Di Marco, P. Thunström, L. Nordström, O. Eriksson, T. Björkman, and J. M. Wills, Comput. Mater. Sci. **55**, 295 (2012).
[22]M. Campagna, E. Bucher, G. K. Wertheim, and L. D. Longinotti, Phys. Rev. Lett. **33**, 165 (1974).
[23]K. Shimada, M. Arita, Y. Takeda, H. Fujino, K. Kobayashi, T. Narimura, H. Namatame, and M. Taniguchi, Surf. Rev. Lett. **9**, 529 (2002).
[24]M. Arita, K. Shimada, Y. Takeda, M. Nakatake, H. Namatame, and M. Taniguchi, Surf. Rev. Lett. **9**, 535 (2002).
[25]A. M. Stewart, Phys. Rev. B **6**, 1985 (1972).
[26]S. K. Malik, Phys. Lett. A **31**, 33 (1970).
[27]J. M. Lawrence, P. S. Riseborough, and R. D. Parks, Rep. Prog. Phys. **44**, 1 (1981).
[28]H. Yamaoka, I. Jarrige, N. Tsujii, M. Imai, J.-F. Lin, M. Matsunami, R. Eguchi, M. Arita, K. Shimada, H. Namatame, M. Taniguchi, M. Taguchi, Y. Senba, H. Ohashi, N. Hiraoka, H. Ishii, and K.-D. Tsuei, Phys. Rev. B **83**, 104525 (2011).
[29]M. Aldén, B. Johansson, and H. L. Skriver, Phys. Rev. B **51**, 5386 (1995).
[30]J. J. Yeh and I. Lindau, At. Data Nucl. Data Tables **32**, 1 (1985).
[31]T. Greber, T. J. Kreutz, and J. Osterwalder, Phys. Rev. Lett. **79**, 4465 (1997).
[32]D. Endoh, T. Goto, A. Tamaki, B. Liu, M. Kasaya, T. Fujimura, and T. Kasuya, J. Phys. Soc. Jpn. **58**, 940 (1989).
[33]M. Arita, K. Shimada, Y. Takeda, M. Nakatake, H. Namatame, M. Taniguchi, H. Negishi, T. Oguchi, T. Saitoh, A. Fujimori, and T. Kanomata, Phys. Rev. B **77**, 205117 (2008).
[34]T. U. Ito, W. Higemoto, K. Ninomiya, H. Luetkens, T. Sugai, Y. Haga, and H. Suzuki, J. Phys. Soc. Jpn. **80**, 033710 (2011).
[35]H. Yamaoka, M. Matsunami, R. Eguchi, Y. Ishida, N. Tsujii, Y. Takahashi, Y. Senba, H. Ohashi, and S. Shin, Phys. Rev. B **78**, 045125 (2008).
[36]E. Vescovo, R. Rochow, T. Kachel, and C. Carbone, Phys. Rev. B **46**, 4788 (1992).
[37]G. Kutluk, M. Nakatake, H. Sumuda, H. Namatame, and M. Taniguchi, Surf. Interf. Anal. **42**, 712 (2010).
[38]H. Yamaoka, I. Jarrige, N. Tsujii, J.-F. Lin, N. Hiraoka, H. Ishii, and K.-D. Tsuei, Phys. Rev. B **82**, 035111 (2010).
[39]M. P. Seah and W. A. Dench, Surf. Interf. Anal. **1**, 2 (1979).
[40]A. Yamasaki, A. Sekiyama, S. Imada, M. Tsunekawa, C. Dallera, L. Braicovich, T.-L. Lee, A. Ochiai, and S. Suga, J. Phys. Soc. Jpn. **74**, 2538 (2005).
[41]G. K. Wertheim and G. Grecelius, Phys. Rev. Lett. **40**, 813 (1978).